J. Fluid Mech. (1998), *vol.* 354, *pp.* 43–67. Printed in the United Kingdom

Equilibrium of liquid drops under the effects of rotation and acoustic flattening: results from USML-2 experiments in Space

By C. P. LEE, A. V. ANILKUMAR, A. B. HMELO AND T. G. WANG

Center for Microgravity Research and Applications, Vanderbilt University, Nashville, TN 37235, USA

(Received 13 January 1997 and in revised form 27 August 1997)

Previous Space-based experiments (Wang *et al.* 1994*a*) showed that a rotating liquid drop bifurcates into a two-lobed shape at a lower critical angular velocity, if it is flattened acoustically by the leviating sound field. In this work, we undertake a systematic experimental study of the effect of acoustic flattening on the rotational bifurcation of a liquid drop. We also look into the complementary effect of rotation on the equilibrium of an acoustically drastically flattened drop. Theoretical models are developed for each of the two effects and then woven into a unified picture. The first effect concerns neutral equilibrium, while the second concerns loss of equilibrium, neither of them involving instability. The theories agree well with the experiments.

1. Introduction

The bifurcation of the equilibrium shape of a rotating drop into two and more lobes was first observed by Plateau (1863), with a liquid drop immersed in a liquid host. Theoretically, Chandrasekhar (1965) calculated the critical rotation rate at which an axisymmetric drop in air or vacuum bifurcates into two lobes. Brown & Scriven (1980) further calculated numerically the equilibrium shapes of the drop after bifurcation. Experimentally, there have been quite a few attempts to test the theory using acoustic levitation (King 1934). Wang *et al.* (1986) found that the critical rotation rate for the two-lobed bifurcation in Spacelab 3 experiments using a three-axis acoustic chamber was lower than expected. Biswas, Leung & Trinh (1991) found a similar discrepancy with the theoretical prediction in a ground-based experimental study using a single-axis acoustic levitator. Rhim, Chung & Elleman (1988) conducted such experiments using an electrostatic levitator instead, and found close agreement with the theory. But the use of electric charge introduces some uncertainty into the validity of the comparison.

Wang *et al.* (1994*a*) repeated the measurements in USML-1 flight experiments, using initially spherical drops as well as those that were acoustically flattened at the poles (Marston 1980; Trinh & Hsu 1986) before rotation. They found that the drops which are free from flattening bifurcate at the theoretically predicted rotation rate. But the drops which are flattened bifurcate at lower rotation rates. Hence the theory of rotational bifurcation has been verified, and the previous discrepancy with the theory explained as due to the flattening.

The question is: how does flattening affect bifurcation? A better understanding of this and related phenomena can contribute to the non-contact techniques for measuring surface tensions (Elleman *et al.* 1985). But a ground-based experiment (Biswas *et al.* 1991) cannot clearly answer this question. According to a remark by

Wang *et al.* (1994*a*), gravity, though small compared with surface tension in the case of small drops, can tip the delicate balance between rotation and surface tension near the bifurcation point. Consequently the drop tends to be spread more horizontally and to become asymmetrical about its equatorial plane as a result of gravity, leading to biased results. This accounts for the difference between the Space-based data of Wang *et al.* (1994*a*) and the ground-based data of Biswas *et al.* (1991). Furthermore, there are always the spatial and temporal limitations in a ground-based study that can be overcome in the microgravity environment of Space, as large drops can be used there. The study of the shift in the bifurcation point due to acoustic flattening is one of the objectives of the recent USML-2 flight experiments.

We are also interested in the complementary effect of rotation on the equilibrium of a drastically flattened drop. It is known that when a drop in air is levitated in a sound field, it is flattened by the acoustic radiation pressure (Marston 1980). The flattening increases with the sound intensity up to a point. Beyond this point, flattening increases with *decreasing* sound intensity, if the latter can occur. Otherwise, the flattened drop loses its equilibrium, expands horizontally, and eventually shatters, being torn apart by the acoustic suction stress at its equator (Lee, Anilkumar & Wang 1991, 1994; Anilkumar, Lee & Wang 1993; Shi & Apfel 1995). The breakup is a case of 'loss of equilibrium,' which means that the equilibrium simply ceases to exist when the system crosses a certain threshold. We have avoided the word 'instability,' which means that an equilibrium basically exists, but it is unstable to certain disturbances.

The purpose of the present work is to study the effect of flattening on the two-lobed bifurcation phenomenon, as well as the effect of rotation on the equilibrium of a flattened drop. Data have been taken systematically in the USML-2 experiments, using drops that were deliberately flattened before rotation was imposed.

Theoretically, the two problems have to be handled differently. The first problem is the effect of acoustic flattening on the rotational two-lobed bifurcation of a drop. The flattening will be treated as a perturbation. The second problem is the effect of rotation on the axisymmetric equilibrium of an acoustically drastically flattened drop. The case of a rotating drop without acoustics has been thoroughly studied by Ross (1968). Our problem including acoustics will be treated numerically without approximation by using a boundary integral technique (Lee *et al.* 1994). At the end the two problems will be put together to give a unified picture, to compare with the experiments.

2. Experimental procedure

The apparatus in USML-2 is the same Drop Physics Module (DPM) used in USML-1, where USML stands for United States Microgravity Laboratory. Since it has been described previously by Wang *et al.* (1994*a*), we shall not repeat the description here. But let us explain briefly the acoustics involved.

Before a drop is deployed, there are three plane standing sound waves along the x-, y- and z-directions of the acoustic chamber. After a drop is deployed, if the drop is small in comparison with the dimensions of the chamber, each sound wave is perturbed by a wavelet scattered from the drop surface to the surroundings with little echo (see Leung *et al.* 1982, for example). The chamber dimension, and therefore the acoustic frequency, in the z-direction is different from those in the x- and y-directions. Thus on the average, the z-wave is not coupled to the x- and y-waves. But the latter are coupled with each other to impose an acoustic torque along the z-direction (Busse & Wang 1981), as well as an acoustic radiation potential in the (x, y)-plane (Lee & Wang 1988) on the drop, both depending on the amplitudes of and the phase difference between the

	ν (cSt)	ρ (gm cm^{-3})	σ (dyn cm^{-1})
Session 1	100	0.962	20.9 ± 0.2
Session 2	350	0.966	21.1 ± 0.2
Session 3	1000	0.968	21.1 ± 0.2

TABLE 1. Properties of the liquids used in the experiments at 25 °C, where the values of ν are nominal values provided by the manufacturer, those of ρ are measured from retained samples of the flight liquids, and those of σ are measured from leftover samples of the flight liquids.

Drop #	Volume (cm^3)	α	Run temp (°C)	Flattening (%)	Ω_c'
Session 1					
1	3.00 ± 0.05	0.19	25.0	~ 0	0.557*
2	3.14 ± 0.05	0.19	25.5	35 ± 2.0	0.448*
3	1.01 ± 0.02	0.13	25.5	18 ± 1.5	0.511*
4	0.92 ± 0.015	0.12	25.5	182 ± 6.0	0.118**
5	2.00 ± 0.02	0.16	26.3	146 ± 5.0	0.165**
Session 2					
1	3.04 ± 0.03	0.19	19.6	~ 0	0.565*
			20.8	19 ± 0.7	0.492*
			21.0	208 ± 6.0	0.0**
2	2.80 ± 0.03	0.18	22.5	120 ± 4.0	0.200**
Session 3					
1	1.31 ± 0.02	0.14	21.0	~ 0	0.563*
			22.1	~ 0	0.564*
			22.5	7.5 ± 1.0	0.536*
2	1.54 ± 0.02	0.15	23.0	28.5 ± 1.3	0.470*
			23.3	102 ± 3.0	0.244***

TABLE 2. Experimental data, where * signifies two-lobed bifurcation, ** signifies axisymmetric loss of equilibrium, and *** signifies axisymmetric loss of equilibrium after a failed attempt at bifurcation.

two waves. Drop rotation is effected along the z-direction by using the torque. The drop is levitated (King 1934) and deformed (Marston 1980) by the sum of the radiation pressure from the z-wave and that from the coupling of the x- and y-waves.

However, acoustic field measurements are not directly used in the data analysis for the following reasons. First, the sound pressure level picked up by each microphone is the combined sound pressure level of more than one wave, such that the amplitude of each wave cannot be evaluated with high accuracy. Secondly, in the idealized situation of the theory, the drop is flattened by a single plane wave. In the experiment, all of the x-, y- and z-waves are needed in practice to keep the drop in position. While it is mainly the z-wave that does the flattening, all three waves inevitably contribute to the deformation of the drop. In order to compare with theory, we have to talk about a single z-wave that is equivalent to the three waves, in the sense that it can give the same deformation. The frequency of the equivalent z-wave is taken as that of the original z-wave, and its amplitude is inferred indirectly from the deformation of the drop.

The experiments were conducted using Dow Corning 200 series silicone oils, with drops of volumes from 1 to 3 cm^3, and viscosities 100, 350 and 1000 cSt (table 1). High viscosities were chosen in order to reduce the relaxation times of the drops between spin-up and equilibrium. Various viscosities were used in order to observe the effects of viscosity on the fission process. But the critical rotation rate at which bifurcation or loss of equilibrium occurs is associated with equilibrium, and is therefore independent

of viscosity. The silicone oils of various viscosities vary little in surface tension and density. An advantage of using silicone oils is that their surface tensions are insensitive to contamination, if there is any.

The drops were deployed using flat-tip injectors (Wang *et al.* 1994*a*). Each drop was acoustically flattened first, before an acoustic torque was imposed to spin up the drop up to and beyond bifurcation. Flattening is measured by $(a/b-1)\times 100\,\%$, where a and b are respectively the equatorial and polar radii of the drop. The spin-up was slow enough to ensure that the drop was close to rigid-body rotation at all times. Tracer particles were used to follow the rotation of the drops, such that a solid-body rotation could be visually recognized when it occurred, and the resulting rotation rate could be measured. Pliolite tracer particles (Goodyear Chemical Co.), about 50–100 μm in size, were mixed with the liquids during preparation.

The experiments were performed in three sessions (tables 1 and 2), corresponding to the three values of viscosity mentioned above. In each run, the initially flattened drop was spun up until one of the following two things happened: the drop bifurcates from an axisymmetric shape into a two-lobed equilibrium shape, which, upon further spin-up, eventually becomes unstable and fissions into two drops (Chandrasekhar 1965; Brown & Scriven 1980); the drop retains its axisymmetric shape as it becomes more flattened, until it loses equilibrium, expands horizontally and shatters (Lee *et al.* 1991, 1994; Anilkumar *et al.* 1993; Shi & Apfel 1995).

We also wanted to look for the effects of viscosity on the fission process, but due to the difficulties involved in dislodging high-viscosity drops from the injector tips, we were able to deploy drops up to about 1000 cSt only.

All data analysis is done using video tape with information available at 60 fields/s. Only drops whose volumes, and whose flattening before rotation, can be estimated accurately are selected for presentation. This requirement means that the selected drops did not have any uncontrolled rotation before the torque was turned on. The uncontrolled rotation often happens to a sample in acoustic levitation (e.g. see Wang *et al.* 1994*b*; Wang, Anilkumar & Lee 1996), but its nature has not been understood.

Let ρ and σ be the density and surface tension of the liquid, and R_0 be the spherical radius of the drop. The size of the drop is specified by $\alpha = kR_0$, where k is the wavenumber ($= 2\pi/$wavelength of the z-wave, where the wavelength $= 2\times$chamber height $= 30.48$ cm) of the sound wave that vibrates along the axis of symmetry of the drop. The quadrupole oscillation frequency of the drop (Lamb 1945) is given by $\omega_0 = (8\sigma/\rho R_0^3)^{1/2}$.

As shown in table 2, the values of the drop size α are all small enough that none of these drops significantly affected the sound field (Leung *et al.* 1982). It follows that the sound amplitude can be considered as constant while the drop went through the spin-up and shape changes. That is also why we consider the axisymmetric loss of equilibrium of a drop through horizontal expansion, but not the possibility that the drop can stay in equilibrium by reducing the sound intensity through a resonant frequency shift (Lee *et al.* 1991, 1994; Anilkumar *et al.* 1993).

The surface tension for each drop is corrected by -0.08 dyn cm^{-1} °C^{-1}, taking into account the temperature during a run, which typically lasted for a few minutes during which the temperature was essentially constant. The measurement errors for the rotation rate Ω and linear dimensions are estimated to be less than 0.5 %. The uncertainty in the estimation for the normalized rotation rate, given by $\Omega^* = \Omega/\omega_0$, is about 2 %, taking into consideration the systematic error in the estimation of ω_0 for each drop (see Wang *et al.* 1994*a*). In the plots that follow, whenever the errors are smaller then the plot symbols, they have not been separately indicated.

3. Experimental results and discussion

For each experiment, the drop size, temperature during the run, the degree of flattening imposed on the initially non-rotating drop, and the clinical rotation rate for breakup are listed in table 2. The experiments are classified into three sessions according to the viscosities of the oils to be used. As we have explained earlier, the breakup can occur through fission at the end of a two-lobed bifurcation, or through the loss of equilibrium of an axisymmetrically flattened drop, depending on the relative strengths of rotation and acoustic flattening.

As we have also noted earlier, the drops we used were small enough, such that the sound intensity that was used to initially flatten a drop can be considered as constant throughout the deformation process of the drop. Hence, there is a one-to-one correspondence between the 'initial flattening' and the constant sound intensity. When we refer to 'initial flattening' in the following, we do not mean that there is no acoustic flattening after rotation starts. When the drop rotates, the constant sound intensity is still there, but the flattening is due to both acoustics and rotation. The contribution to flattening from the constant sound intensity is not constant but depends on the shape of the drop.

Let us define R^* as the maximum equatorial radius R scaled by R_0, for either the axisymmetric or two-lobed shape. One way to present the evolution of a drop is to plot R^* versus the normalized rotation rate Ω^*, for a given initial flattening. Note that dynamic processes, including the fission of the drop beyond two-lobed bifurcation, and the horizontal expansion of the drop after axisymmetric loss of equilibrium, cannot strictly be characterized by these two parameters. But our primary interest is equilibrium. Therefore, dynamic processes branching out from equilibrium will be conveniently and loosely considered as extensions of the equilibrium, and thereby described in terms of the same parameters.

In figure 1 we show such a plot for session 1 experiments with 100 cSt oil. For reference purposes, we have also drawn the (solid) theoretical curve describing the deformation of an initially spherical drop due to rotation alone (Chandrasekhar 1965; Brown & Scriven 1980). The curve goes from left to right, representing the deformed but axisymmetric equilibrium shape of the drop. But it turns upward and backward at the critical rotation rate $\Omega_c^* = 0.56$, leading to the familiar bifurcation branch for the two-lobed equilibrium shape of the drop (Brown & Scriven 1980).

For a flattened drop, the experimental curve that goes from left to right similarly represents its axisymmetric deformation due to increasing rotation rate. As expected, this part of the curve shifts upward from its counterpart in the reference curve, as the initial flattening increases.

For each flattened drop, the curve similarly turns backward and upward from the axisymmetric curve, at a critical rotation rate depending on the initial flattening. But the nature of the transition also depends on the initial flattening as follows. The experimental data are classified into two clusters: the one on the right-hand side leads to two-lobed bifurcation, while the one on the left-hand side leads to axisymmetric loss of equilibrium.

From the cluster on the right-hand side, it is clear that the critical rotation rate for bifurcation decreases with initial flattening. The bifurcation branch also rises more vertically and crosses the reference curve at some point. The greater the initial flattening is, the more pronounced these tendencies are. The reason is simply that each lobe of the two-lobed shape is flattened by the acoustic radiation pressure from an almost spherical shape into an approximately oblate shape, with the axis of symmetry

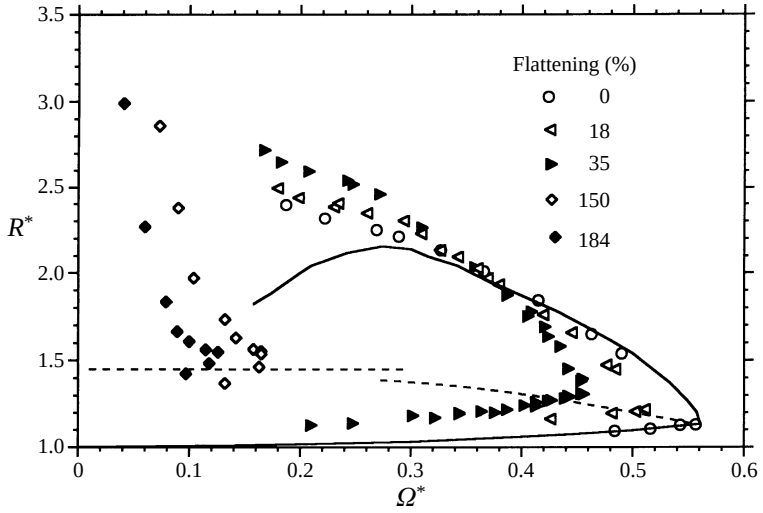

FIGURE 1. R^* versus Ω^* for 100 cSt drops from session 1. The solid curve is from Brown & Scriven (1980), in which the lower part corresponds to an axisymmetric drop before bifurcation, and the upper part corresponds to the same drop adopting a two-lobed equilibrium shape after bifurcation. The data points on the right corresponds to two-lobed bifurcation perturbed by acoustic flattening. The data points on the left represents loss of axisymmetric equilibrium under the influence of rotation. The dashed lines represent the theories in the present work (the dashed horizontal line corresponds to curve ed and the dashed slanted curve corresponds to ba in figure 12).

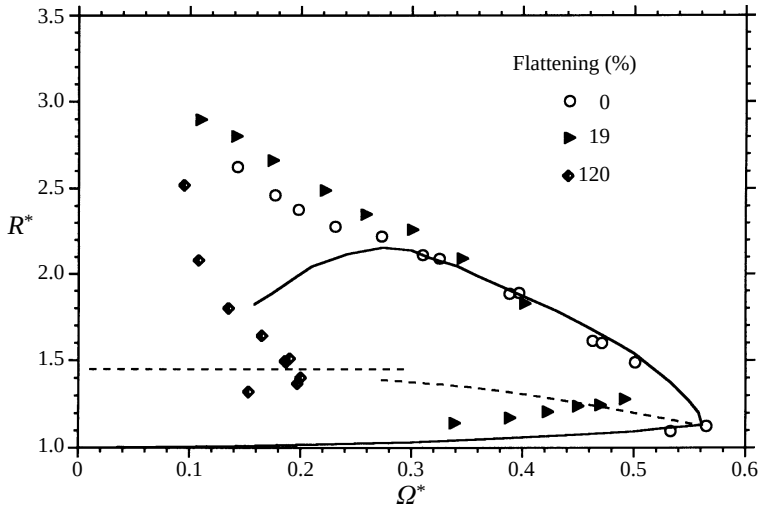

FIGURE 2. R^* versus Ω^* for 350 cSt from session 2. The description is similar to that for figure 1.

being parallel to the axis of rotation, effectively increasing R^*. The neck between the two lobes is relatively narrow, such that the effect of the acoustic radiation stress is less important there. The two-lobed bifurcation path ends at the fission point, beyond which the drop follows the curve that approximately obeys $\Omega^* R^{*2} = \text{constant}$. This means conservation of angular momentum, considering the two lobes as two spherical masses flying off tangentially after the ligament between them can no longer hold them together in equilibrium. The curve ends at some R^* where the ligament between the two lobes breaks.

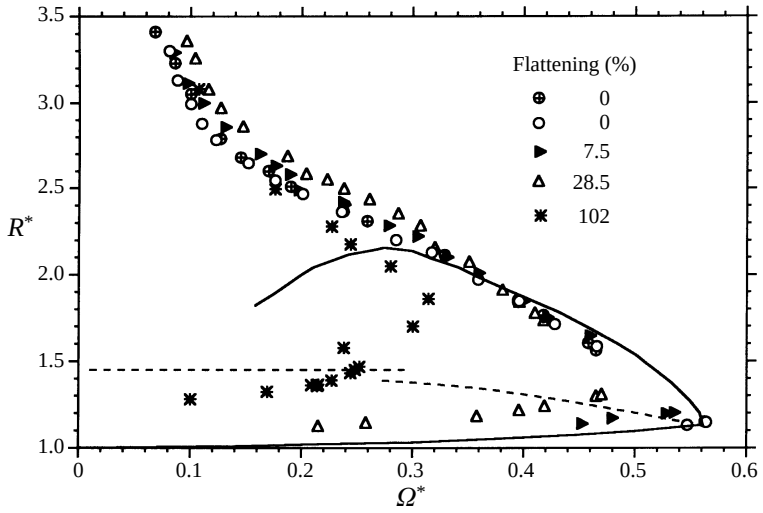

FIGURE 3. R^* versus Ω^* for 1000 cSt drops from session 3. The 102% flattening drop tries but fails to bifurcate at $\Omega^* = 0.25$, retains its axisymmetric shape, picks up more angular velocity, and finally loses axisymmetric equilibrium at around $\Omega^* = 0.32$. The other drops all bifurcate. The dashed lines have been explained in the caption of figure 1.

For the cluster on the left-hand side, where the drops suffer from greater initial flattening, there is no bifurcation: a drop simply loses equilibrium beyond the critical rotation rate. The curve that branches out from the axisymmetric curve represents not equilibrium, but the dynamic process of axisymmetric horizontal expansion due to the acoustic suction stress at the equator of the drop (Lee *et al.* 1991, 1994; Anilkumar *et al.* 1993; Shi & Apfel 1995), with a little help from the centrifugal force due to the rotation. The curve also approximately obeys $\Omega^* R^{*2} =$ constant, which again means conservation of angular momentum, considering that the mass of the drop is concentrated near the equator like a ring.

In figure 2, we plot the R^*, Ω^* curves for the 350 cSt drops of session 2, and can describe them similarly to those of session 1. With the higher viscosity, the fission curve can extend to higher R^*, because the higher viscosity can keep the ligament between the two lobes intact for a bit longer before breaking.

In figure 3 we show the data for the 1000 cSt drops of session 3. Some of the drops were used repeatedly because they could be re-captured by the acoustic potential well after fission, made possible by the strong viscous effect on the separation motion between the two lobes. The drop can reach a high R^* before breaking, again due to viscosity, but with the two lobes carrying little momenta in separation because of the heavy viscous dissipation. However, the fission curve still exhibits conservation of angular momentum, because the viscous force is not an external force, and so it cannot change the angular momentum.

A special feature in figure 3 is the behaviour of the 102% flattening drop. The drop lies between the regime where the drop bifurcates and that where the drop loses axisymmetric equilibrium. At the rotation rate of about 0.25, it tries to bifurcate, but fails to do so, retaining its axisymmetric shape, and loses equilibrium at a higher rotation rate.

The main results of the experiments are shown in figure 4, where we plot the data, from both USML-1 and USML-2, in the form of critical rotation rate versus initial acoustic flattening. The points stand for drops of different sizes (table 2), but the values

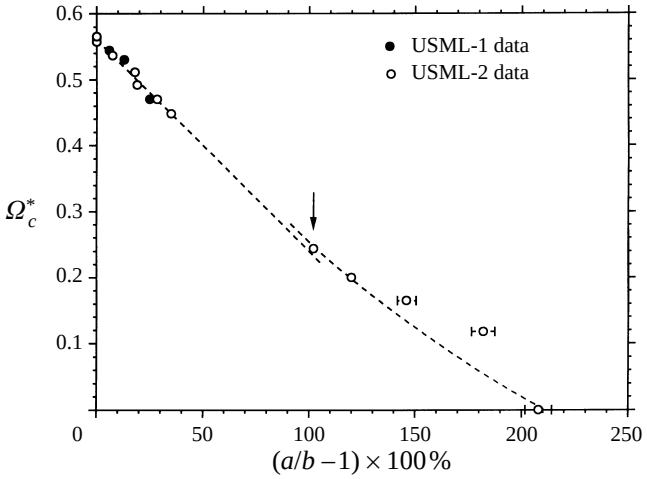

FIGURE 4. Critical rotation rate versus flattening. The drop sizes can be found in table 2, and can be considered to be asymptotically small, acoustically speaking. The cluster on the left-hand end represents two-lobed bifurcation perturbed by flattening. The other data points to the right represent axisymmetric loss of equilibrium under the influence of rotation. The 102% drop in figure 3 is highlighted here by an arrow. The dashed lines represent the theories in the present work (see figure 13).

(*a*)

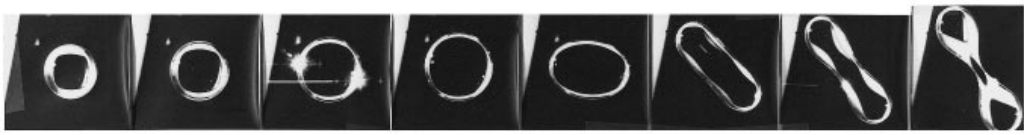

(*b*)

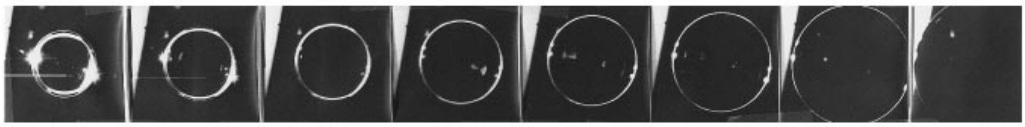

FIGURE 5. Photographs showing (from left to right) the top views of a drop undergoing (*a*) rotation bifurcation, and (*b*) axisymmetric loss of equilibrium. Sequence (*a*) represents equilibrium shapes at slowly increasing angular momentum. Sequence (*b*) is a dynamic process that takes place suddenly and rapidly beyond a critical point.

of α are small enough such that the asymptotical limit $\alpha \to 0$ can be considered. The cluster of data on the left-hand end represents two-lobed bifurcation perturbed by acoustic flattening. The other data further to the right represent loss of axisymmetric equilibrium under the influence of rotation.

In figure 5(*a*), we show a sequence of photographs of the top views of a drop undergoing rotational bifurcation at slowly increasing angular momentum. In figure 5(*b*), we show a similar sequence for a drop undergoing sudden axisymmetric loss of equilibrium.

4. Rotational bifurcation of a slightly acoustically flattened drop

4.1. *Definition of the problem*

Consider a small liquid drop levitated at the pressure node of a plane standing sound wave, in the absence of gravity. Let the drop rotate around the axis that is parallel to the direction of the sound vibration. The problem in this study is to calculate the two-lobed bifurcation of the drop, if it is slightly flattened by the acoustic radiation pressure from the sound field.

Inevitably, the problem involves a preliminary calculation of the bifurcation point without the sound wave, but this point has already been calculated accurately a few times (Chandrasekhar 1965; Brown & Scriven 1980; Luyten & Callebaut 1983). Considering also that the focus of the present study is the effects of the acoustic perturbation on the bifurcation of the drop, we choose to derive the bifurcation point in a lowest-order approximation. For the unperturbed bifurcation point, the approach is less accurate. But the approach allows easy incorporation of acoustics later. Furthermore, this approach will prove to be adequate for the correction to the bifurcation point due to acoustics. It also provides a clear physical picture for the whole phenomenon.

4.2. *Axisymmetric equilibrium*

Let us consider a drop of radius R_0, density ρ, and surface tension σ, rotating along the z-axis with angular velocity Ω, in the absence of acoustics. The hydrostatic pressure inside the drop is given in spherical coordinates by

$$P = P_0 + \tfrac{1}{2}\rho\Omega^2 r^2 \sin^2\theta, \tag{4.1}$$

where P_0 is constant, r is the radial coordinate, and θ is the polar angle. Let the drop shape be described by

$$f(\theta) = R_0[1 - \gamma P_2(\theta)], \tag{4.2}$$

where γ is assumed to be small, and P_n for $n = 1, 2, 3, \ldots$ are Legendre polynomials, neglecting terms of $O(\gamma^2)$ inside the square bracket. For equilibrium, the normal stress difference across the drop surface has to be balanced by surface tension. By setting the ambient pressure to zero, this condition leads to the Young–Laplace equation

$$P = \sigma \boldsymbol{\nabla} \cdot \boldsymbol{n}, \tag{4.3}$$

where $\boldsymbol{n}$ is the normal unit vector pointing away from the drop surface. Substituting (4.1) and (4.2) into (4.3) we have

$$\gamma = \tfrac{2}{3}\Omega^{*2}, \tag{4.4}$$

where $\Omega^* = (\rho\Omega^2 R_0^3/8\sigma)^{1/2}$ is the normalized rotation rate, ignoring terms of $O(\Omega^{*4})$ in the lowest-order approximation.

4.3. *Energy principle*

Let us now look for the situation in which the axisymmetric drop can stay in neutral equilibrium, when its surface suffers from a non-axisymmetric two-lobed perturbation at a constant angular momentum L. In other words, we want to find the two-lobed bifurcation point, at which the perturbation does not oscillate or grow in time.

We need to find the point at which the second variation of the energy of the drop with respect to the perturbation is zero. Since the perturbation is imposed at constant angular momentum, the energy to be considered should be identified with the Hamiltonian of the drop. In general, if the axisymmetric or non-axisymmetric drop is in equilibrium, its energy is given by

$$E = E_s + E_r, \tag{4.5}$$

where E_s is its surface energy and E_r is its rotational energy. The surface energy is given by

$$E_s = \sigma \int_S \mathrm{d}a, \tag{4.6}$$

in which the integral is the area of the drop surface S. The rotational energy is given by

$$E_r = \frac{L^2}{2I}, \tag{4.7}$$

in which

$$I = \int_V \rho r^2 \sin^2\theta \, \mathrm{d}\boldsymbol{x} \tag{4.8}$$

is the moment of inertia of the drop, the integration being over its volume V. The angular velocity is given by $\Omega = L/I$.

Let the drop start with an axisymmetric shape characterized by $L = L_c$ and $I = I_c$, where the subscript c represents the critical axisymmetric state at which bifurcation is expected. Then Ω has the value of $\Omega_c = L_c/I_c$ when bifurcation occurs. With the perturbation, I changes by δI, Ω changes by δQ, E_s changes by δE_s, E_r changes by δE_r, and E changes by δE, while L remains constant. The constant of conservation of angular momentum for the perturbation requires that

$$\delta L = I_c \, \delta\Omega + \Omega_c \, \delta I = 0. \tag{4.9}$$

From (4.7) and (4.9), the change in rotational energy is

$$\delta E_r = -\tfrac{1}{2}\Omega_c^2 \, \delta I. \tag{4.10}$$

In order for the shape to stay in equilibrium while perturbed

$$\delta E = \delta E_s + \delta E_r = 0. \tag{4.11}$$

4.4. *Two-lobed bifurcation*

Let the shape of the perturbed drop be described by

$$F(\theta, \phi) = R[1 - (\gamma + \delta\gamma) P_2(\theta) + \epsilon P_2^2(\theta) \cos 2\phi], \tag{4.12}$$

where ϕ is the azimuthal angle, $\epsilon \ll 1$ represents the perturbation, $P_2^2 = 3\sin^2\theta$ is an associated Legendre function that describes the two-lobed feature, and $\delta\gamma$ is the correction in γ due to the introduction of ϵ for the following reason. We have neglected terms of $O(\gamma^2)$ and $O(\epsilon^2)$ inside the square bracket. When ϵ is applied, the moment of inertia I changes by δI, such that according to (4.9), the angular velocity Ω changes by $\delta\Omega$. It follows from (4.4) that γ also changes by $\delta\gamma$.

The quantity I_c for the unperturbed drop is determined from (4.8) and (4.2):

$$I_c = \frac{8\pi\rho R_0^5}{15}(1 + \gamma), \tag{4.13}$$

neglecting terms of $O(\gamma^2)$ inside the bracket. The quantity I for the perturbed drop is similarly determined from (4.8) and (4.12). Comparing the two results, we find

$$\delta I = \frac{8\pi\rho R_0^5}{15}\left(\delta\gamma + \frac{132}{7}\epsilon^2\right). \tag{4.14}$$

Putting (4.13) and (4.14) into (4.9), using (4.4), and rearranging, we find

$$\frac{\delta\Omega}{\Omega_c} = \frac{\delta\gamma}{2\gamma} = -\frac{132}{7}\epsilon^2 \tag{4.15}$$

to the lowest-order approximation in γ.

As seen in (4.10), δE_r is proportional to Ω_c^2, and therefore according to (4.4) is proportional to γ. Substituting (4.14) into (4.10), and using $\delta\gamma \sim \gamma\epsilon^2$ from (4.15), we obtain

$$\delta E_r = 4\pi R_0^2 \sigma\left(-\frac{352}{35}\Omega_c^{*2}\epsilon^2\right), \tag{4.16}$$

where $\Omega_c^* = (\rho\Omega_c^2 R_0^3/8\sigma)^{1/2}$ is the normalized critical rotation rate, to the lowest-order approximation in γ.

The surface energy for the unperturbed drop is determined from (4.2) and (4.6). The surface energy for the perturbed drop is similarly determined from (4.12) and (4.6). Comparing the two results, we find the change in surface energy as

$$\delta E_s = 4\pi R_0^2 \sigma\left(\frac{24}{5}\epsilon^2\right), \tag{4.17}$$

to the lowest-order approximation in γ.

Substituting (4.16) and (4.17) into (4.11), we have the total change in energy as

$$\delta E = 4\pi R_0^2 \sigma\left[\left(\frac{24}{5} - \frac{352}{35}\Omega_c^{*2}\right)\epsilon^2\right] = 0. \tag{4.18}$$

On the right-hand side of the first equality, the coefficient of ϵ^2 is the second variation of E with respect to the perturbation. For bifurcation, we use the second equality to set the coefficient to zero, such that

$$\Omega_c^* = \sqrt{\frac{21}{44}} = 0.69, \tag{4.19}$$

with an error of $O(\gamma)$. If the rotation rate is lower, δE is positive such that the perturbation is oscillatory. If the rotation rate is higher, then δE is negative and the perturbation grows in time.

This reproduces the essential physics of the bifurcation problem. However, compared with the known accurate value of 0.56 for Ω_c^*, our value is too high by 23 %. Given the extent of our simplification, the inaccuracy is not surprising. But recall that our real objective is to study the effects of slight acoustic flattening on bifurcation. We shall therefore look for a relative shift in the bifurcation point from the known accurate unperturbed value of Ω_c^* rather than its absolute value.

4.5. *Axisymmetric equilibrium of a rotating drop slightly flattened by acoustics*

The sound wave under consideration has a wavelength that is much longer than the dimension of the drop, and a frequency that is much larger than the capillary frequency of the drop. The sound wave does not interact with the drop directly at the first order, since the drop cannot respond to the acoustic time scale, but it can affect the drop indirectly through its steady radiation pressure.

In a gas medium of density ρ_0 and speed of sound c_0, let the incident acoustic pressure be given by $p_i' = A\sin(kz)\exp(-i\omega t)$, where A is the amplitude, k is the wavenumber, z is the position relative to the pressure node, $\omega = kc_0$ is the frequency

in rad s^{-1}, and t is time. Let us consider the long-wave limit $\alpha = kR_0 \ll 1$ and let the drop be at the pressure node. If the drop is non-rotating, it is flattened by the acoustic radiation pressure (Marston 1980) such that its shape becomes $f(\theta) = R_0[1-\beta P_2(\theta)]$, where $\beta = 3B_a/32 \ll 1$, in which $B_a = A^2 R_0/\sigma\rho_0 c_0^2$ is the acoustic Bond number, neglecting α^2.

If the drop is rotating, then in place of (4.2), we have a superposition of small deformations due to rotation and acoustics:

$$f(\theta) = R[1-(\gamma+\beta)\,P_2(\theta)]. \tag{4.20}$$

In (4.20), β represents the radiation pressure on a spherical drop. Actually, the sound field should be distorted through scattering by the rotational deformation of the drop, such that β should have a correction. But in this calculation, acoustics is considered as a perturbation, such that the correction due to the rotational deformation is a perturbation of the perturbation, and is thus neglected.

4.6. *Acoustic radiation pressure on a two-lobed drop*

For the sound field, while the axisymmetric deformation of the drop due to rotation is neglected as we have just said, the non-axisymmetric two-lobed deformation at bifurcation should be considered, for reasons which will become clear in the next subsection. Here, we shall calculate the scattered field from the slightly two-lobed shape and the associated radiation pressure. For the present purpose, the two-lobed shape is accordingly written as a simpler version of (4.12):

$$G(\theta,\phi) = R[1+\epsilon P_2^2(\theta)\cos 2\phi]. \tag{4.21}$$

Let the incident wave be $p_i' = p_i \exp(-\mathrm{i}\omega t)$, where $p_i = A\sin(kz)$. Let the scattered wave be $p_s' = p_s \exp(-\mathrm{i}\omega t)$. The total wave $p' = p_i' + p_s' = p\exp(-\mathrm{i}\omega t)$, satisfies the Helmholtz equation $\nabla^2 p + k^2 p = 0$, and the boundary condition $\partial p/\partial n = 0$ on the drop surface described by (4.21). The particle velocity is given by $\boldsymbol{u}' = \boldsymbol{u}\exp(-\mathrm{i}\omega t)$, where $\boldsymbol{u} = (\mathrm{i}\omega\rho_0)^{-1}\,\boldsymbol{\nabla} p$. The radiation pressure on the drop surface is given by (King 1934)

$$P_a = \frac{\langle p'^2\rangle}{2\rho_0 c_0^2} - \frac{\rho_0}{2}\langle \boldsymbol{u}'\cdot\boldsymbol{u}'\rangle, \tag{4.22}$$

where $\langle\ \rangle$ means the time average over an acoustic cycle.

We shall consider a perturbation about the spherical surface $r = R_0$ instead of dealing directly with the flattened surface. We shall consider the wave scattering from the spherical surface, subjected to a modified boundary condition obtained by expanding the original boundary condition in ϵ. The boundary condition is thus rewritten as

$$\left(\frac{\partial p_s}{\partial r}\right)_{r=R_0} + \left(\frac{\partial^2 p_s}{\partial r^2}\right)_{r=R_0} \epsilon R_0\, P_2^2 \cos 2\phi = -\left(\frac{\partial p_i}{\partial r}\right)_{r=R_0} - \left(\frac{\partial^2 p_i}{\partial r^2}\right)_{r=R_0} \epsilon R_0\, P_2^2 \cos 2\phi. \tag{4.23}$$

The incident wave is expanded as (Morse & Feshbach 1953)

$$p_i = \sum_{n=1}^{\infty}{}' A\mathrm{i}^{n-1}(2n+1)\,j_n(kr)\,P_n(\theta), \tag{4.24}$$

where the j_n are spherical Bessel functions, and $\sum'$ means that the summation is over odd integers, as a result of the drop sitting at $z = 0$. Let the scattered wave be written as

$$p_s = \sum_{n=0}^{\infty} A_n\, h_n^{(1)}(kr)\,P_n(\theta) + \epsilon\left[\sum_{j=2}^{\infty} C_j\, h_j^{(1)}(kr)\,P_j^2(\theta)\right]\cos 2\phi, \tag{4.25}$$

where the $h_n^{(1)}$ are spherical Hankel functions of the first kind, and the second term on the right is a summation of all the modes that have the factor $\cos(2\phi)$, to conform to the two-lobed shape in (4.21).

Let us substitute (4.24) and (4.25) into (4.23) and equate equal powers of ϵ. At $O(\epsilon^0)$, we have the incident wave plus the wave scattered by the spherical drop, and at $O(\epsilon^1)$, we have the additional wave scattered by the two-lobed perturbation. The total acoustic pressure on the spherical surface is, to the lowest order in kR_0,

$$(p)_{r=R_0} = \frac{3}{2}(kR_0)\, A\cos\theta + \frac{3}{20}(kR_0)\,\epsilon A P_3^2(\theta)\cos 2\phi. \tag{4.26}$$

The component of the particle velocity in the θ-direction is given by

$$(u_\theta)_{r=R_0} = \frac{3\mathrm{i}}{2}\frac{A}{\rho_0 c_0}[\sin\theta - 3\epsilon\sin\theta P_2(\theta)\cos 2\phi]. \tag{4.27}$$

According to (4.22), both p and u_θ lead to contributions of $O(\epsilon)$ to the radiation pressure. The velocity component in the ϕ-direction is of $O(\epsilon)$. The normal velocity on the spherical surface, according to (4.23), is of $O(\epsilon)$. These two, according to (4.22), lead to contributions of $O(\epsilon^2)$ to the radiation pressure and are neglected. The radiation pressure is then

$$P_a = \frac{9}{16}\frac{A^2}{\rho_0 c_0^2}[-\sin^2\theta + 6\epsilon\sin^2\theta P_2(\theta)\cos 2\phi]. \tag{4.28}$$

It can be checked that the first term on the right-hand side leads to the acoustic deformation β, if we balance the axisymmetric part of the radiation pressure with surface tension in a Young–Laplace equation.

4.7. *Effects of acoustics on a two-lobed bifurcation*

According to (4.20), the deformations γ due to rotation and β due to acoustics are simply additive at the lowest order. Since the changes in rotational and surface energies, as given at the lowest order of γ by (4.16) and (4.17), respectively, do not depend on γ, the acoustic effect does not appear in the energy changes at this order either. Hence if (4.11) or (4.18) is still valid, then at the lowest order of γ, acoustics does not affect the two-lobed bifurcation. We shall show below that acoustics should be included in the energy equation.

Everything that we have derived is still valid at the lowest order of γ, except for (4.11), which should be replaced by

$$\delta E = \delta E_s + \delta E_r + \delta E_a = 0, \tag{4.29}$$

where δE_a is the work done by the drop against the radiation pressure in a shape perturbation. Equation (4.18) will be changed accordingly later. Since we are only concerned with the axisymmetric drop at the point of two-lobed bifurcation, the drop cannot suffer from an external torque due to acoustics, but it does experience push or pull from the radiation pressure when it changes shape, which means that it has to do work at its surface.

The work done is the product of the radiation pressure and the surface displacement, integrated over the drop surface. According to (4.21) this is

$$\delta E_a = \int_S \mathrm{d}s\, P_a(\epsilon R_0\, P_2^2\cos 2\phi). \tag{4.30}$$

According to (4.30), it is clear that only the non-axisymmetric part of the radiation pressure in (4.28) contributes, which is why we need to consider scattering by the two-lobed shape in the previous subsection. Substituting (4.28) into (4.30) we obtain

$$\delta E_a = 4\pi R_0^2 \sigma \left(-\frac{27}{35} B_a \epsilon^2 \right). \tag{4.31}$$

Putting (4.16), (4.17) and (4.31) into (4.29), we have approximately, in place of (4.19)

$$\Omega^*_{c,a} = \sqrt{\frac{21}{44}} \left(1 - \frac{9}{112} B_a \right). \tag{4.32}$$

Defining $\Delta\Omega^* = \Omega^*_{c,a} - \Omega^*_c$, we have from (4.32) and (4.19),

$$\frac{\Delta\Omega^*}{\Omega^*_c} = -\frac{9}{112} B_a. \tag{4.33}$$

Let a and b be respectively the equatorial and polar radius of the acoustically flattened drop before rotation, such that $a = R(1+\beta/2)$ and $b = R(1-\beta)$. The acoustic deformation as defined by Wang *et al.* (1994*a*) is $a/b-1$, which is approximately $3\beta/2$ for small β. Hence by relating B_a to β and then to the acoustic deformation, we have more conveniently,

$$\frac{\Delta\Omega^*}{\Omega^*_c} = -\frac{4}{7} \left(\frac{a}{b} - 1 \right), \tag{4.34}$$

which does not depend on the accurate value of Ω^*_c.

4.8. *Discussion*

According to the speculation of Wang *et al.* (1994*a*), since the drop at the bifurcation point is still axisymmetric, the radiation pressure cannot exert a torque on it, so that the critical angular momentum at which bifurcation occurs is not expected to be affected by the sound field. But when the drop is flattened by acoustics axisymmetrically, its moment of inertia increases. Therefore, with the same critical angular momentum, the critical rotation rate at which bifurcation occurs decreases.

Let us re-examine this previous hypothesis in view of our present result. First, by replacing γ with $\gamma+\beta$ in (4.13) in the same way that (4.2) is replaced by (4.20), and using $\beta = 3B_a/32$, the moment of inertia I_c of the axisymmetric drop at the bifurcation point without acoustics is shifted by $\Delta I = (1/20)\pi\rho R_0^5 B_a$ due to acoustics. The angular momentum $L_c = I_c \Omega_c$ at the bifurcation point without acoustics is shifted by $\Delta L = \Omega_c \Delta I + I_c \Delta\Omega$ due to acoustics, where $\Delta\Omega$ is the dimensional form of $\Delta\Omega^*$ in (4.33). Using the above expression for ΔI, (4.13) for I_c, and (4.33) for $\Delta\Omega$, we find that $\Delta L/L_c = -0.0092 B_a$. Since $\Delta\Omega/\Omega = -0.080 B_a$ according to (4.33), the relative shift in the critical angular momentum is much smaller. The critical angular momentum is thus essentially unaffected by acoustics, as the previous hypothesis assumes.

It is still true that no external torque is involved in the shift in the critical rotation rate. But the previously neglected external normal forces does play a role, and the key to the understanding of the phenomenon lies not in the angular momentum but in the energy. According to (4.28), around the equator of the drop, the non-axisymmetric part of the acoustic radiation pressure, which contributes to the energy balance, is negative where the surface is displaced outward and positive where the surface is displaced inward. (This is akin to the situation in which the radiation pressure at the equator of an acoustically flattened drop becomes more negative, as the radius of

curvature at the equator becomes smaller (Lee *et al.* 1991).) It follows that the work done by the surface is negative. Consequently, the radiation pressure makes it easier for the drop to become more two-lobed, allowing bifurcation to occur at a lower rotation rate.

The theory is for a single acoustic wave, whereas in the experiments there are three waves in three orthogonal directions. Each of these waves exerts an acoustic radiation stress on the drop. In order to relate the theory to experiments, it is necessary to consider a single effective wave in the z-direction, giving the drop a net deformation of a/b. Therefore (4.34) should in practice be used instead of (4.33).

However, this argument is not applicable for the case of a single acoustic wave. It is then necessary to justify the choice between (4.33) and (4.34). For small acoustic disturbance, the two equations are equivalent. But for larger acoustic disturbance, which we intend to extrapolate our result to, they do deviate from each other. In principle, of course, one can determine which equation is more valid by carrying the calculation to higher orders of the acoustic perturbation. But we choose to make an educated guess as follows.

The parameter B_a in (4.33) is akin to the radiation stress and thus the force balance at the surface. The parameter $(a/b-1)$ in (4.34) represents the surface deformation and hence, in the case of neutral stability, is more akin to the energy of the rigidly rotating system. As indicated in (4.29), and as we have discussed above, this problem is about energy, and so the choice of (4.34) is more appropriate.

5. The effects of rotation on an acoustically drastically flattened drop

5.1. *Definition of the problem*

Let us consider the same incident sound wave as in §4. Only axisymmetric scattering is considered this time. When the drop is levitated in air by the acoustic radiation pressure of the wave (King 1934), it is also flattened in the axial direction by the radiation pressure (Marston 1980). The degree of flattening can be measured by $R^* = R/R_0$, where R is the equatorial radius of the drop after it has been flattened. The acoustic radiation pressure is characterized by the acoustic Bond number $B_a = A^2 R_0/\sigma\rho_0 c_0^2$. For small deformations (Marston 1980), B_a increases with R^*. For larger deformations (Lee *et al.* 1991, 1994; Anilkumar *et al.* 1993; Shi & Apfel 1995), B_a rises to a peak value that depends on the drop size $\alpha = kR_0$, at $R^* \approx 1.45$. At the peak, at the equator of the flattened drop where the curvature is high there is a delicate balance between surface tension which pulls inward, and the acoustic radiation stress which pulls outward. If the sound intensity is increased beyond this critical point, the drop cannot stay in equilibrium and has to expand horizontally and eventually shatter. But the sound intensity can in fact decrease beyond this point, due to the detuning and consequent power loss of the acoustic levitator, if the drop with its flattened shape is large enough compared with the acoustic wavelength to block the acoustic path significantly (Leung *et al.* 1982). If that is the case, then beyond this point the drop can be further flattened in decreasing sound intensity, such that B_a decreases with R^* (Lee *et al.* 1991, 1994; Anilkumar *et al.* 1993). In this study, we are only concerned with the rising part of the B_a versus R^* curve, since small drops in a large levitator cannot present a significant blockage, and thus cannot survive beyond the peak of the B_a, R^* curve without shattering there.

The ground-based experimental B_a, R^* curves (Anilkumar *et al.* 1993) are consistently somewhat above the theoretically predicted ones (Lee *et al.* 1994). In a ground-based experiment, where only small drops can be used, a higher sound pressure

level is needed to deform a drop than in Space. Such a sound wave has many harmonics, but only the lowest harmonics are effective in deforming the drop. These lowest harmonics contribute to an effective sound pressure level that is lower than the total one. Thus the discrepancy between theory and experiment is due to relating B_a to the total sound pressure level rather than the effective one. Moreover, the ground-based experiments were conducted using a single-axis ultrasonic levitator, in which the sound field falls off laterally, and the drop is levitated slightly below a pressure node due to gravity. It has been speculated (Lee *et al.* 1994) that these also contribute to the differences between the experimental B_a, R^* curves and the theoretically predicted ones. The USML-2 experiments using a three-axis acoustic chamber have the advantage over the ground-based experiments that the sound field does not fall off laterally, and that there is no gravity.

In order to facilitate a better comparison between theory and experiment, we shall introduce rotation into a previous boundary integral formulation for the flattened drop (Lee *et al.* 1994). We shall numerically calculate the effects of the rotation on the stability of the flattened drop. No approximation is needed, except that the possibility for the two-lobed bifurcation of the drop at a critical rotation rate (Brown & Scriven 1980) is neglected. The latter will be taken into consideration when we put the two problems together in comparison with experiment.

Therefore in this part, we want to calculate the equilibrium shape of the drop under the influence of the acoustic radiation pressure, at a sound intensity ranging from zero to the maximum value beyond which the drop cannot stay in equilibrium, given a rotation rate Ω for the drop. In other words, we want to find the shift of the B_a, R^* curve as a function of the rotation rate.

5.2. *Formulation*

In the absence of gravity, the drop is located at $z = 0$. Let the total sound field be represented by the acoustic pressure $p' = \mathrm{Re}[p(\boldsymbol{x})\exp(-\mathrm{i}\omega t)]$, where p is real, depending only on the position $\boldsymbol{x}$, and satisfying the Helmholtz equation $\nabla^2 p + k^2 p = 0$. The wave consists of the incident wave $p_i = A\sin(kz)$ which we have mentioned earlier, and the scattered wave p_s, such that $p = p_i + p_s$. It satisfies the boundary conditions that $\boldsymbol{n}\cdot\nabla p = 0$ on the drop surface, where $\boldsymbol{n}$ is the normal unit vector on the surface pointing away from the drop, and that p_s approaches zero at large distance from the drop.

The sound wave depends on the drop shape, which depends on the acoustic radiation pressure, which in turn depends on the sound wave. Hence both the sound wave and the drop shape are parts of the solution of the problem. Lee *et al.* (1994) dealt with this problem in a self-consistent way by using a boundary integral technique. It consists of an iteration scheme in which the sound wave is calculated given the drop shape, the drop shape is recalculated given the resulting acoustic radiation pressure, and the sound field is recalculated given the new drop shape, and so on.

Given a drop shape, the sound field on the drop surface is given by

$$p_s(\boldsymbol{x}) = \frac{1}{2\pi}\mathrm{PV}\int_S \mathrm{d}S\left[p_s(\boldsymbol{y})\frac{\partial G(\boldsymbol{y}-\boldsymbol{x})}{\partial n} + G(\boldsymbol{y}-\boldsymbol{x})\frac{\partial p_i(\boldsymbol{y})}{\partial n}\right], \tag{5.1}$$

where S is the surface of the drop, n is the distance along the outward-pointing unit vector $\boldsymbol{n}$, $G(\boldsymbol{y}-\boldsymbol{x}) = \exp(\mathrm{i}k|\boldsymbol{y}-\boldsymbol{x}|)/|\boldsymbol{y}-\boldsymbol{x}|$ is the Green's function for the Helmholtz equation, which has a singularity at $\boldsymbol{y} = \boldsymbol{x}$, and PV denotes that the principal value of the integral be taken owing to the singularity.

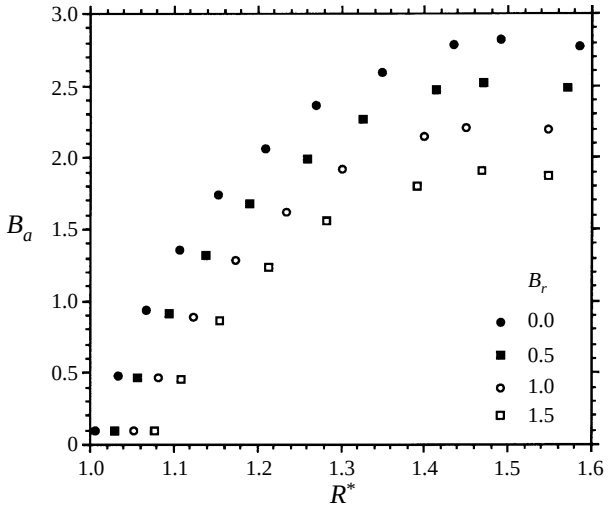

FIGURE 6. Calculated B_a versus R^* for $\alpha = 0.5$ at various B_r.

The radiation pressure is given by

$$P_a = \frac{\langle p'^2 \rangle}{2\rho_0 c_0^2} - \frac{\rho_0 \langle \boldsymbol{u} \cdot \boldsymbol{u} \rangle}{2}, \tag{5.2}$$

where $\langle\ \rangle$ denotes a time average over an acoustic cycle, and

$$\boldsymbol{u} = \mathrm{Re}[\boldsymbol{\nabla} p \exp(-\mathrm{i}\omega t)/\mathrm{i}\omega\rho_0]$$

is the acoustic particle velocity. As far as the acoustic oscillation is concerned, the drop surface can be considered as rigid, such that $\boldsymbol{u}$ only has a tangential component there.

The drop shape is determined by the Young–Laplace equation, which balances surface tension, acoustic radiation pressure and centrifugal force:

$$\sigma \boldsymbol{\nabla} \cdot \boldsymbol{n} = P_I - P_a + \tfrac{1}{2}\rho\Omega^2 r^2, \tag{5.3}$$

where P_I is the internal pressure that is uniform inside the drop. The whole calculation is the same as that of Lee *et al.* (1994), except that P_I is replaced by $P_I + \rho\Omega^2 r^2/2$ everywhere. Specifically, the changes are made in the Young–Laplace equation (5.3), and in the expression for P_I in terms of the acoustic radiation stress and the curvature of the drop at the equator (equation (15) of Lee *et al.* 1994).

Following Lee *et al.* (1994), the dimensionless forms of the equations depend on the drop size $\alpha = kR_0$, the acoustic Bond number $B_a = A^2 R_0/\sigma\rho_0 c_0^2$, the degree of flattening $R^* = R/R_0$, and in addition, the rotational Bond number $B_r = \rho\Omega^2 R_0^3/\sigma$.

5.3. *Procedure and results*

The detailed numerical procedure can be found in Lee *et al.* (1994) and will not be described here. The first part of the procedure is to calculate the B_a, R^* curve to the peak, for each given α which ranges from 0.01 to 1.0, and for each given B_r which ranges from 0 to 1.5, looking for a pattern. The typical variation of the curve with B_r for a given α is given by figure 6, which shows a set of non-intersecting B_a, R^* curves. It is noted that the critical value R^*_{cr} of R^*, where the curve is maximum, is approximately constant at about 1.45, irrespective of B_r. But the maximum value $B_{a,c}$ of B_a decreases with B_r.

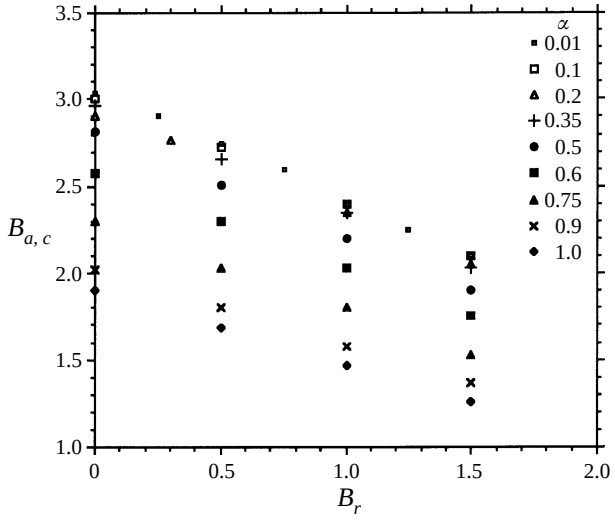

FIGURE 7. Calculated $B_{a,c}$ versus B_r for various α.

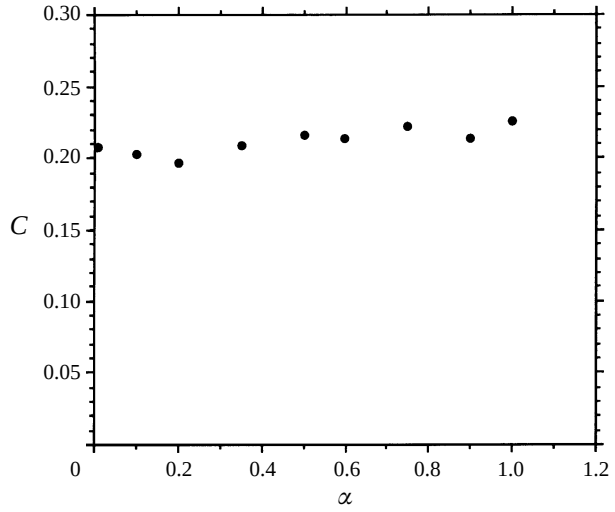

FIGURE 8. Calculated C versus α.

Basing on this observation, the second part of the procedure is to find the variation of $B_{a,c}$ with B_r for each given α. The results are shown in figure 7, which plots $B_{a,c}$ versus B_r for various values of α. It can be seen that the change ΔB_a in $B_{a,c}$ is proportional to B_r for each α.

In the third part of the procedure, the fractional change is found by best-fitting each set of data points in figure 7 with a straight line, and normalizing the change with the unperturbed $B_{a,c}$. We find that

$$\frac{\Delta B_a}{B_{a,c}} = -CB_r, \tag{5.4}$$

where the proportionality constant C is a function of the drop size α. But when C is plotted against α in figure 8, it can be seen that C is approximately 0.21 and is essentially independent of α.

5.4. *Discussion*

We have found above that the position R_c^* of the peak of the B_a, R^* curve is independent of the rotation rate. However, Anilkumar *et al.* (1993) in their ground-based experiments found that the peak shifts slightly to higher R^* with increasing rotation rate.

It is noted that in the latter experiment, the rate of increase of sound intensity was constant and did not slow down when the drop approached the peak of the B_a, R^* curve. The constant increase in sound intensity is expressed by $\mathrm{d}B_a/\mathrm{d}t$ being finite, where t is time. The peak of the B_a, R^* curve is characterized by $\mathrm{d}R^*/\mathrm{d}B_a \to \infty$. Since $\mathrm{d}R^*/\mathrm{d}B_a = (\mathrm{d}R^*/\mathrm{d}t)/(\mathrm{d}B_a/\mathrm{d}t)$, a finite $\mathrm{d}B_a/\mathrm{d}t$ means an infinite $\mathrm{d}R^*/\mathrm{d}t$. A large $\mathrm{d}R^*/\mathrm{d}t$ in turn means a flattening that is too fast for the viscous relaxation of the rotation of the drop, which is estimated to take R^2/ν. Thus the drop could not attain a rigid-body rotation near the peak, as required by the theory, and the disagreement is not surprising.

6. Unified picture and comparison with experiment

6.1. *Hybrid model*

From the experimental point of view, given the initial acoustic flattening of a small drop, we want to find the critical rotation rate for bifurcation or loss of equilibrium. This requires us to put the two theories together to form a unified picture, together with some numerical work in interpolation.

Let us do the following calculation for $\alpha = 0.25$, which can be considered as asymptotically small, acoustically speaking. In figure 9, we plot B_a versus R^* for various values of B_r, including the calculated data points and the best fits. It can be seen that the peak values of B_a occur at a constant $R_c^* \approx 1.45$, irrespective of B_r.

Truncating the curves at $R^* = R_c^*$, figure 9 is transformed into figure 10, in which we plot B_r versus R^* for various values of B_a, again including the calculated data points and the best fits.

As we have explained earlier, since the drop is acoustically small, the sound intensity is not affected by the presence of the drop. Hence the sound intensity can be evaluated from the deformation before rotation starts. In other words, there is a one-to-one correspondence between B_a and the initial a/b. In figure 11, we show this correspondence for the $\alpha = 0.25$ drop.

Using the relation in figure 11, as well as the relation $B_r = 8\Omega^*2$, figure 10 is transformed into figure 12, in which we plot R^* versus Ω^* for various initial values of a/b. Let us temporarily ignore the possibility of two-lobed bifurcation. The curve for $a/b = 1$ is the familiar one representing the deformation as a function of the rotation rate alone (Chandrasekhar 1965; Brown & Scriven 1980). For any initial a/b, if Ω^* increases from zero, R^* increases until it reaches R_c^*, where the drop loses it axisymmetric equilibrium and shatters. The horizontal line edc on the (R^*, Ω)-plane marks the position $R^* = R_c^*$ where the drop loses its equilibrium. In particular, the point e is the critical point for the non-rotating drop (Lee *et al.* 1991, 1994; Anilkumar *et al.* 1993; Shi & Apfel 1995).

Now let us impose (4.34), which represents two-lobed bifurcation, onto figure 12. The equation determines the bifurcation point on the R^*, Ω^* curve for each initial a/b. The locus of these bifurcation points is the curve ab. In particular, point a is the familiar bifurcation point for the drop that is free from acoustics (Chandrasekhar 1965; Brown & Scriven 1980). We end the curve at point b, because it becomes

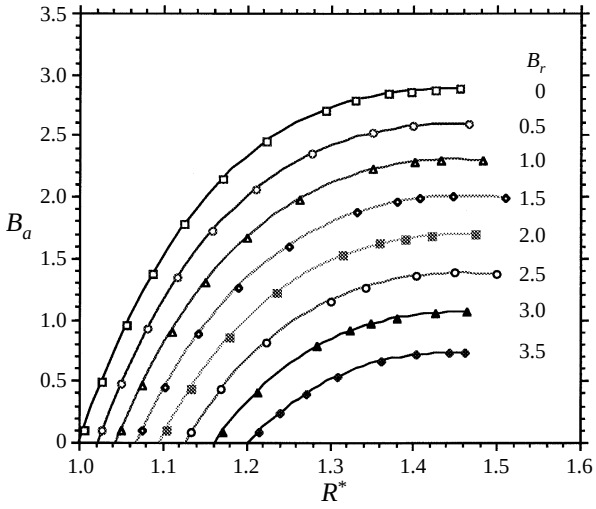

FIGURE 9. Calculated B_a versus R^* for $\alpha = 0.25$ at various B_r.

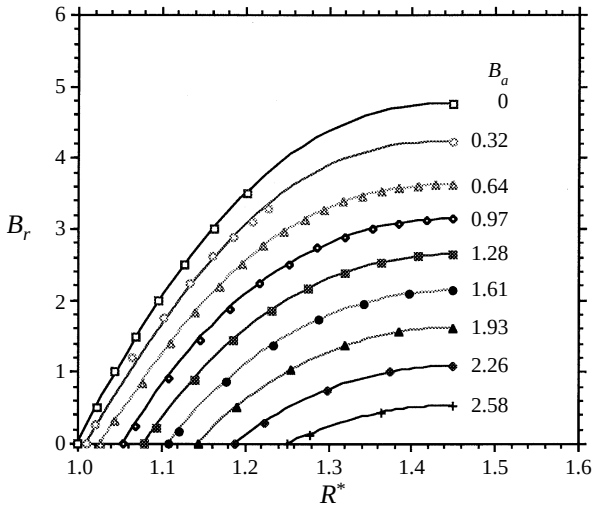

FIGURE 10. Calculated B_r versus R^* for $\alpha = 0.25$ at various B_a.

increasingly difficult to get more R^*, Ω^* curves beyond this point, by interpolation of the finite number of data points given in figure 9. But it also happens, as seen in figure 12, that the points b and d are in the neighbourhood in which the regimes represented by ab and cde merge.

The composite plot answers the question we have posed at the beginning of this section as follows. Given a drop that is flattened acoustically before rotation, we locate the point on the R^*-axis that corresponds to the initial a/b. As the rotation rate Ω^* increases, we follow the R^*, Ω^* curve for that initial a/b to the right. Then one of the two following things can happen. If the magnitude of the initial a/b is small enough, the R^*, Ω^* curve can cut the curve ab such that the drop undergoes a two-lobed bifurcation. On the other hand, if the magnitude of the initial a/b is large enough, the R^*, Ω^* curve can cut the line de such that the drop ends up losing its axisymmetric equilibrium and shatters. The segment cd of the line cde lies behind the curve ab, can never be cut before two-lobed bifurcation occurs, and is thus irrelevant.

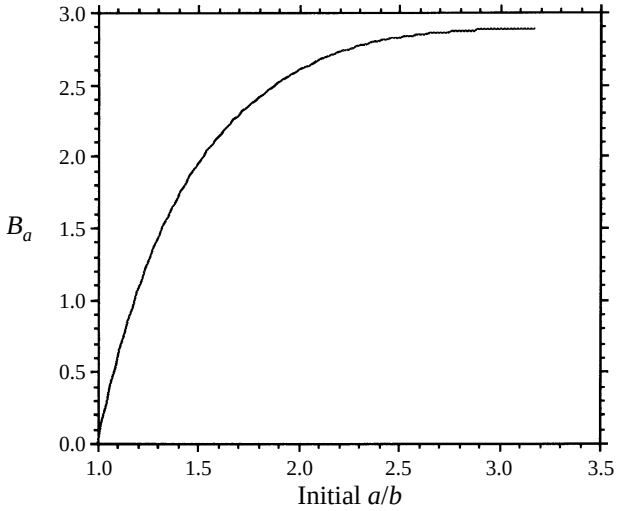

FIGURE 11. Calculated B_a versus initial a/b for $\alpha = 0.25$.

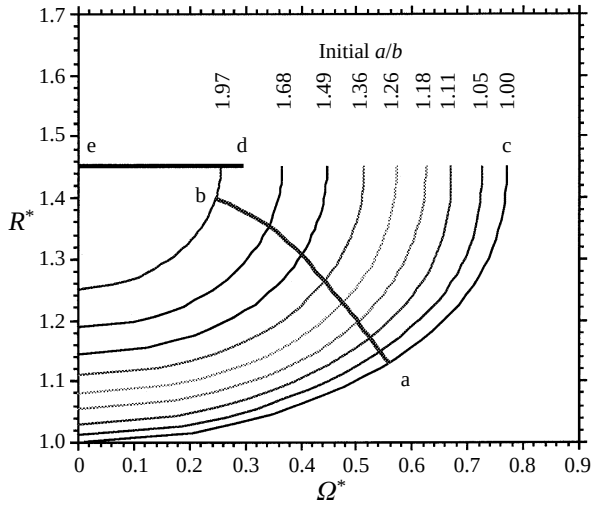

FIGURE 12. Calculated R^* versus Ω^* for various initial a/b for $\alpha = 0.25$. The curve ab is the locus of bifurcation points for various R^*, Ω^* curves. The line cde marks the maximum R^* beyond which the drop loses axisymmetric equilibrium and shatters.

This picture is better expressed by plotting the critical rotation rate Ω_c^* versus $(a/b-1)\times 100\,\%$ as in figure 13. The curves corresponding to ab and cde in figure 12 are again shown here. It can be seen that the curve ab for two-lobed bifurcation, which is a straight line according to (4.34), almost connects with the curve de for axisymmetric loss of equilibrium, which is no longer a straight line in this representation, around the points b and d. It is clear that with a little matching, the two curves can merge smoothly with each other.

Note that the curve de cuts the $(a/b-1)\times 100\,\%$ axis at a finite angle between 0° and 90°. This can be proved as follows. Let us denote the point $R^* = R_c^*$ and $B_r = 0$, near the bottom right corner in figure 10, as X. Let us consider a contour of constant B_a near and around X (similar to the one for $B_a = 2.58$). The decrease ΔB_a in B_a along the line

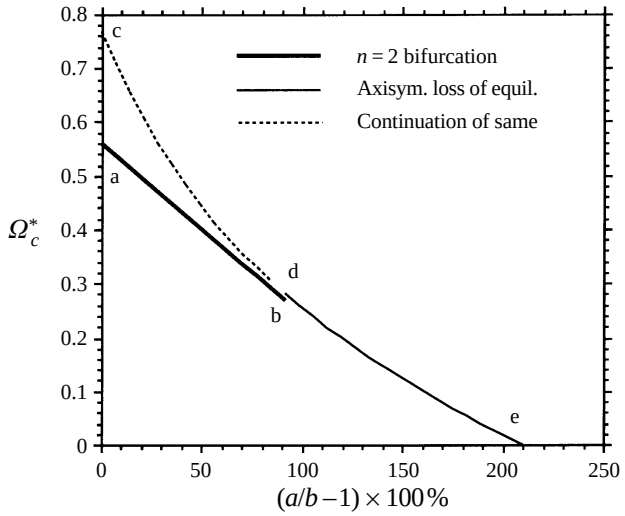

FIGURE 13. Calculated critical rotation rate Ω_c^* versus $(a/b-1)\times 100\,\%$, with line ab covering two-lobed bifurcation, curve de covering axisymmetric loss of equilibrium, and cd being the continuation of de.

parallel to the B_r axis from X to the contour is given by $(\Delta B_a)_1 \propto B_r$, according to (5.4), or $(\Delta B_a)_1 = C_1 \Omega^{*2}$, since B_r is proportional to Ω^{*2}. The decrease ΔB_a in B_a along the line antiparallel to the R^*-axis from X to the contour is given by $(\Delta B_a)_2 = C_2(\Delta R^*)^2$, where ΔR^* is the displacement in the negative R^*-direction. Obviously, $(\Delta B_a)_1 = (\Delta B_a)_2$ since the drop is from X to the same contour. Therefore we have $\Omega^* = (C_2/C_1)^{1/2}\Delta R^*$. Furthermore, since the liquid drop is acoustically small, its shape is close to ellipsoidal even at maximum flattening ($R^* = R_c^*$). Therefore we can use the ellipsoidal approximation $a/b = R^{*3}$, such that ΔR^* is related to the change $\Delta(a/b)$ in a/b by $\Delta R^* = \Delta(a/b)/3R_c^{*2}$. Finally, combining this with the earlier expression for Ω^*, we have $\Omega^* = (C_2/C_1)^{1/2}\Delta(a/b)/3R_c^{*2}$. This proves that the curve de comes out from the $(a/b-1)\times 100\,\%$ axis at a finite angle.

6.2. *Comparison with experiments and discussion*

The curves ab and de in figure 12 have been imposed on figures 1–3 from USML-2. It can be seen that the agreement is good except for the 102 % drop from figure 3 (see § 3). For this particular drop, the two-lobed bifurcation point at $\Omega^* = 0.25$ is as predicted. Then the drop backs off from bifurcation and suffers from more flattening until it loses axisymmetric equilibrium at $\Omega^* = 0.32$. But the latter point does not lie along the axisymmetric loss of equilibrium line.

Similarly, the curves ab and de in figure 13 have been imposed on figure 4 from both USML-1 and USML-2. It can be seen more clearly than the agreement for two-lobed bifurcation, according to the cluster of data points on the left-hand end, is excellent. The agreement for the data points for axisymmetric loss of equilibrium, according to the data points further to the right, is better for smaller a/b than for larger a/b. This is a bit surprising, considering that the model for the two-lobed bifurcation of a flattened drop involves a lot of simplification, whereas the theory for the axisymmetric equilibrium of a drop is exact for the idealized situation of one single plane wave whose vibration direction is along the rotation axis.

The discrepancy for larger a/b can be attributed to the following. While two-lobed bifurcation is about energy, axisymmetric equilibrium is about the force balance

among surface tension, acoustic stress, and centrifugal force at the highly curved equator, characterized by the parameter B_a (Lee *et al.* 1991, 1994; Anilkumar *et al.* 1993; Shi & Apfel 1995). It follows that it is B_a, rather than a/b, that is the more natural parameter to be plotted against Ω^* in figure 4 or 13, in the regime for axisymmetric loss of equilibrium. On the other hand, it is not practical to measure B_a because it is meant for one wave while the system had three waves, and because the sound pressure level is much more difficult to measure accurately than a/b. Furthermore, with the three waves, the one-to-one correspondence between B_a and a/b as shown in figure 11 is blurred, since each value of a/b corresponds to three B_a values along the three axes. It is true that the B_a along the axis of flattening is the most important. But the situation is complicated by the fact that the region under consideration is near the point $(a/b-1)\times 100\,\% = 210$, which corresponds to the peak of the $B_a, a/b$ curve in figure 11.

With this background, the discrepancy is explained as follows. Each value of a/b corresponds to approximately the B_a along the axis of flattening. But this value of B_a is changed a bit after being corrected for the presence of the B_a along the other two axes. There is a further correction due to the previously neglected small power loss, as a result of the detuning effect of the flattened drop. The corrected B_a in turn has to correspond to a corrected a/b. Near the peak of the $B_a, a/b$ curve in figure 11, the value of a/b is very sensitive to B_a. Hence a little correction to B_a leads to a large correction to a/b. In other words, the 'true' a/b can be different from the observed one by a large correction.

But as seen in figure 11, as a/b moves away from the peak, it becomes less sensitive to B_a. Therefore, we can see that the agreement between theory and experiment improves as the data points move away from the maximum $(a/b-1)\times 100\,\%$ point in figure 4. Allowing for the aforementioned inaccuracy associated with a/b, and except for the 102% drop from figure 3, the experimental data are quite supportive of the theory.

The $(a/b-1)\times 100\,\% = 102\,\%$ drop takes a special position in figure 4. It is represented by its failed two-lobed bifurcation point $\Omega^* = 0.25$, although its demise was due to an axisymmetric loss of equilibrium. The latter event, at $\Omega^* = 0.32$, corresponds to a point that is significantly above the theoretical curve.

It is noted that the 102% drop is in the neighbourhood where the curve for two-lobed bifurcation, and the curve for axisymmetric loss of equilibrium, are expected to merge in figure 13. This means that the drop was very sensitive to little disturbances, which could easily push it over from one regime to the other. Hence the drop should have bifurcated at $\Omega^* = 0.25$ in the absence of disturbances. It is amazing that the model (4.34) is applicable even when the flattening is so large.

What is not clear is why the drop did not lose equilibrium at $R^* = R_c^* = 1.45$ like other similar drops, but at some higher R^*, after it found itself in the regime of axisymmetric loss of equilibrium.

7. Conclusion

Previous experiments (Wang *et al.* 1994*a*) showed that acoustic flattening lowers the two-lobed bifurcation point of a rotating drop. In this work, we have conducted systematic experimental and theoretical studies of the effect of acoustic flattening on rotational bifurcation, which concerns neutral stability. We have also considered the other extreme regime of the effect of rotation on the equilibrium of an acoustically drastically flattened drop, which concerns loss of equilibrium. Theoretical models have

been developed for the two effects and then put together to explain the whole situation. The theoretical results agree well with the experiments.

In summary, we have explored a situation in which a regime of neutral stability overlaps with a regime of equilibrium on the verge of collapsing, in the context of a rotating drop subjected to acoustic flattening. Away from the overlap region, equilibrium does not collapse where two-lobed bifurcation occurs. Likewise, there is no two-lobed bifurcation where equilibrium is near collapse. This is just a matter of which scenario has the chance to happen first for the given conditions. The borderline case of the 'confused' 102% drop in figure 3 might be worthy of further study.

The analysis and theory described in this paper were carried out at the Center for Microgravity Research and Applications at Vanderbilt University under contract with the National Aeronautics and Space Administration.

REFERENCES

Anilkumar, A. V., Lee, C. P. & Wang, T. G. 1993 Stability of an acoustically levitated and flattened drop: an experimental study. *Phys. Fluids* A **5**, 2763–2774.

Biswas, A., Leung, E. W. & Trinh, E. H. 1991 Rotation of ultrasonically levitated glycerol drops. *J. Acoust. Soc. Am.* **90**, 1502–1507.

Brown, R. A. & Scriven, L. E. 1980 The shape and stability of rotating liquid drops. *Proc. R. Soc. Lond.* A **371**, 331–357.

Busse, F. H. & Wang, T. G. 1981 Torque generated by orthogonal acoustic waves–theory. *J. Acoust. Soc. Am.* **69**, 1634–1638.

Chandrasekhar, S. 1965 The stability of a rotating liquid drop. *Proc. R. Soc. Lond.* A **286**, 1–26.

Elleman, D. D., Wang, T. G., Trinh, E. H. & Croonquist, A. P. 1985 Contactless measurement of physical properties. *NASA Technol. Brief* NPO-15839.

King, L. V. 1934 On the acoustic radiation pressure on spheres. *Proc. R. Soc. Lond.* A **147**, 212–240.

Lamb, H. 1945 *Hydrodynamics*, 6th edn. Dover.

Lee, C. P., Anilkumar, A. V. & Wang, T. G. 1991 Static shape and instability of an acoustically levitated liquid drop. *Phys. Fluids* A **3**, 2497–2515.

Lee, C. P., Anilkumar, A. V. & Wang, T. G. 1994 Static shape of an acoustically levitated drop with wave-drop interaction. *Phys. Fluids* **6**, 3554–3566.

Lee, C. P. & Wang, T. G. 1988 Acoustic radiation potential on a small sphere due to two orthogonal standing waves. *J. Acoust. Soc. Am.* **83**, 2459–2461.

Leung, E., Lee, C. P., Jacobi, N. & Wang, T. G. 1982 Resonance frequency shift of an acoustic chamber containing a rigid sphere. *J. Acoust. Soc. Am.* **72**, 615–620.

Luyten, P. & Callebaut, D. K. 1983 Stability of rotating liquid drops. I. Uncharged drops. *Phys. Fluids* **26**, 2359–2367.

Marston, P. L. 1980 Shape oscillation and static deformation of drops and bubbles by modulated radiation stress – theory. *J. Acoust. Soc. Am.* **67**, 15.

Morse, P. M. & Feshbach, H. 1953 *Methods of Theoretical Pbysics*. McGraw Hill.

Plateau, J. A. F. 1863 Experimental and theoretical researches on the figures of equilibrium of a liquid mass withdrawn from the action of gravity. *Ann. Rep. Board of Regents of the Smithsonian Institution*, pp. 270–285. Washington, DC.

Rhim, W. K., Chung, S. K. & Elleman, D. D. 1988 Experiments on rotating charged liquid drops. *Drops and Bubbles, 3rd Intl Colloq., Monterey, CA, 1988* (ed. T. G. Wang). *AIP Conf. Proc. 197*.

Ross, D. K. 1968 The shape and energy of a revolving liquid mass held together by surface tension. *Austral. J. Phys.* **21**, 823–835.

Shi, W. T. & Apfel, R. E. 1995 Instability of a deformed liquid drop in an acoustic field. *Phys. Fluids* **7**, 2601–2607.

Trinh, E. H. & Hsu, C. J. 1986 Equilibrium shapes of acoustically levitated drops. *J. Acoust. Soc. Am.* **79**, 1335.

WANG, T. G., ANILKUMAR, A. V. & LEE, C. P. 1996 Oscillations of liquid drops: results from USML-1 experiments in Space. *J. Fluid Mech.* **308**, 1–14.

WANG, T. G., ANILKUMAR, A. V., LEE, C. P. & LIN, K. C. 1994*a* Bifurcation of rotating liquid drops: results from USML-1 experiments in Space. *J. Fluid Mech.* **276**, 389–403.

WANG, T. G., ANILKUMAR, A. V., LEE, C. P. & LIN, K. C. 1994*b* Core-centering of compound drops in capillary oscillations: observations on USML-1 experiments in Space. *J. Colloid Interface Sci.* **165**, 19–30.

WANG, T. G., TRINH, E. H., CROONQUIST, A. P. & ELLEMAN, D. D. 1986 Shapes of rotating free drops: Spacelab experimental results. *Phys. Rev. Lett.* **56**, 452–455.